Characterising Driver Chest Loading in Front Crash Tests Using Pressure Mat Measurements

Matthew L. Brumbelow

Abstract For belted drivers in frontal crashes, the chest remains the most frequently injured region at AIS≥3, yet existing dummy metrics fail to predict these injuries accurately. This study investigates whether high-speed pressure mat measurements can provide improved insight into chest loading. Pressure data were collected from 87 moderate-overlap crash tests and three sled tests using an XSensor mat positioned to cover all six ribs of a Hybrid III 50M dummy. Data were used to calculate total rib force, forces on upper and lower ribs, belt-path loading, and a force-imbalance metric quantifying how unevenly loads are distributed across the ribcage.

Across current vehicles, total rib forces ranged from 2.4 kN to 5.9 kN, with wide variation in upper- and lower-rib loading and weak correlation between them ($r^2 = 0.28$). Sled tests showed that shoulder-belt tension strongly influenced upper-rib forces, while a knee bolster reduced lower-rib forces. The force-imbalance metric correlated closely with belt-path loading and highlighted differences in how restraint systems distribute similar overall forces across the chest.

By capturing both magnitude and distribution of rib loading, the pressure mat metrics reveal restraint system differences not evident in deflection or belt tension measures and may support future improvements in chest injury assessment.

Keywords Crashworthiness, Dummies, Restraint systems, Thoracic injury, XSensor.

I. INTRODUCTION

Frontal crashes accounted for 60% of passenger vehicle occupant fatalities in the USA in 2023 [1]. Drivers restrained by a seat belt and airbag in a frontal crash sustain serious chest injuries more often than serious injuries to other body regions [2]. Crashworthiness improvements have resulted in lower overall risk of serious and fatal injury [3-4]. However, unlike the risk to other body regions, overall crash test ratings have not been directly linked to the risk of driver chest injury [5].

Previous research using both field crashes and tests involving post-mortem human subjects (PMHS) has indicated that chest injury risk can be reduced by a combination of three strategies: distributing the restraint force over a wider area of the ribs [6-9]; increasing load through the lower extremities and clavicle [9-12]; and reducing the force on the lower ribs relative to the upper ribs [10][13]. These approaches may overlap when considering a specific countermeasure. For example, a knee bolster or knee bolster airbag may provide an alternative load path while also reducing the lower rib force relative to the upper ribs by reducing pelvis excursion. While these three strategies are not comprehensive (e.g. vehicles with longer crush zones have lower risk [14]), they provide a framework for assessing existing or alternative physical tools used in crashworthiness evaluations.

The rib design and deflection measurement systems for both the Hybrid III (HIII) and THOR dummies were developed based on biofidelity targets that do not account for any of the three restraint strategies listed above. The primary loading condition involving a pendulum impact centred on the sternum was designed to represent loading by a steering-wheel hub to the ribs of a driver unrestrained by a seat belt, airbag or knee bolster. Today's restraint systems produce loads that differ in location, magnitude, duration and rate. As discussed in detail in previous studies [5][14-17], these disparities may explain why it has been challenging to demonstrate a direct link between dummy measures and the risk of serious chest injury in field crashes, even when considering THOR's additional measurement capabilities and more sophisticated thorax design compared with HIII. While field crash injuries have been linked to measures of upper shoulder-belt tension in crash tests [14][17], on its own this metric does not capture how factors like belt geometry, airbag characteristics or knee bolster loading may affect chest

M. L. Brumbelow (e-mail: mbrumbelow@iihs.org; tel: +1-434-985-4600) is a Principal Research Engineer at the Insurance Institute for Highway Safety in Virginia, USA.

loads and resulting injury risk [9].

A direct measurement of dummy chest loads that can quantify force distribution, encourage alternative load paths, and measure differences in loads on the lower and upper ribs could help identify restraint improvements that could benefit thousands of frontal-crash-involved occupants each year. One potential tool for capturing these data is the XSensor high-speed impact system consisting of a pressure sensor mat and data logger. The sensor mat records a two-dimensional pressure profile at frequencies up to 3,300 Hz. Since 2023, IIHS has been using the system to determine dynamic belt position for the rear-seated HIII 5th percentile female in the moderate-overlap front crash test [18]. The belt position measurements are used in combination with the recorded potentiometer deflection to assign a chest protection rating for the rear dummy. While the chest injury rating for the HIII 50th percentile male (HIII-50M) dummy in the driver position has been unchanged, an XSensor pressure mat has been used to record pressure data in many tests to research the possibility of developing an alternative chest injury rating procedure. This study describes the recorded pressure data and proposes new metrics that align with protection principles identified from field crashes and PMHS tests.

II. METHODS

Crash Tests and Sled Tests

The tests described in this study consist of 87 full-scale crash tests and three sled tests, all using a HIII-50M dummy in the driver position. All crash tests were 40% overlap tests with an impact speed of 64 km/h, following the IIHS moderate-overlap test protocol [18]. Most of these were conducted as part of the IIHS crashworthiness evaluation program of 2021–2025 model year vehicles, but five 2004–2012 model year vehicles were tested to provide comparison data from earlier designs. All test vehicles in the study are listed in Table AI in Appendix A.

Three sled tests were conducted to provide a baseline without any airbag load sharing and to isolate the effects of different force limiter thresholds and knee bolster loading on the pressure data (Table I). The dummy was positioned in a driver seat from a small car and restrained with a three-point shoulder belt using representative driver belt geometry. The same seat was used for all three tests. The seat was structurally reinforced to limit deformation during loading and rebound that could affect repeatability of dummy positioning and kinematics. The seat back was reinforced by bolting the top of the frame to steel tubing attached to the sled, and the seat pan frame was cast in rigid polyurethane foam (density of 190 kg/m^3). The seat belt was replaced after each test, and belts with two different force limiter thresholds were used. The retractor-mounted pretensioner was fired at 28 ms in all tests. For two tests, a contoured, rigid steel knee bolster was placed in contact with the dummy's lower legs to minimise pelvis excursion (Fig. 1, *left*). All three tests used the same acceleration pulse, representing the longitudinal component of a typical 64 km/h moderate-overlap crash test (Fig. 1, *right*). The maximum delta-V for the sled tests was 70 km/h, which matches the mean longitudinal delta-V for all moderate-overlap crash tests conducted in 2025 (n=64).

TABLE I

SLED TESTS

Test	Target force limiter threshold	Knee bolster
1	4 kN	Yes
2	5.5 kN	Yes
3	5.5 kN	No

XSensor Pressure Mat

Pressure data were recorded using an XSensor pressure mat (XSENSOR Technology Corporation, Calgary, Canada) with 64 columns and 60 rows of pressure-sensing cells. With each cell measuring 5.08 mm on each side, the overall dimensions of the pressure sensing area were 325 x 305 mm. Data were recorded at 2,000 Hz. As shown in Fig. 2, the mat was attached to the dummy underneath the T-shirt using tape so that the pressure-sensing area fully overlapped the six ribs of the dummy. Post-test inspections and CMM measurements throughout the series of tests did not indicate relative motion between the sensor and dummy. Pressure data from cells located over the rigid clavicle and shoulder assembly were not used for analyses.

Even after excluding the sensing area over the clavicle, tests had pressure measurements for around 2,000 individual cells, allowing a wide range of possibilities for characterising rib loading. Several metrics were developed using the estimated force, which was calculated by multiplying the pressure in individual cells by the cell area and then summing all relevant cells. In addition to the total force on the ribs, the force on the upper three and lower three ribs was calculated separately (Fig. 2). Individual cells were assigned to these groups based on CMM measurements of the XSensor and dummy taken before each test. Cells were also grouped by whether or not they fell under the belt path, allowing an estimate of the restraint balance between the belt vs airbag. For each test, an initial belt-path estimate was generated by an algorithm that detected the largest absolute pressure transitions between adjacent cells in the same row at the time of maximum total force on the ribs. The resulting belt path was then reviewed visually to ensure that the belt edges were captured by lines linking the largest positive and negative transition points in each row. In a small number of tests, the transitions at peak force time did not produce an unambiguous belt path; in these cases, the nearest time step yielding a consistent definition was used. Review of pressure-map videos indicated minimal belt-path movement between pretensioner deployment and peak total force.

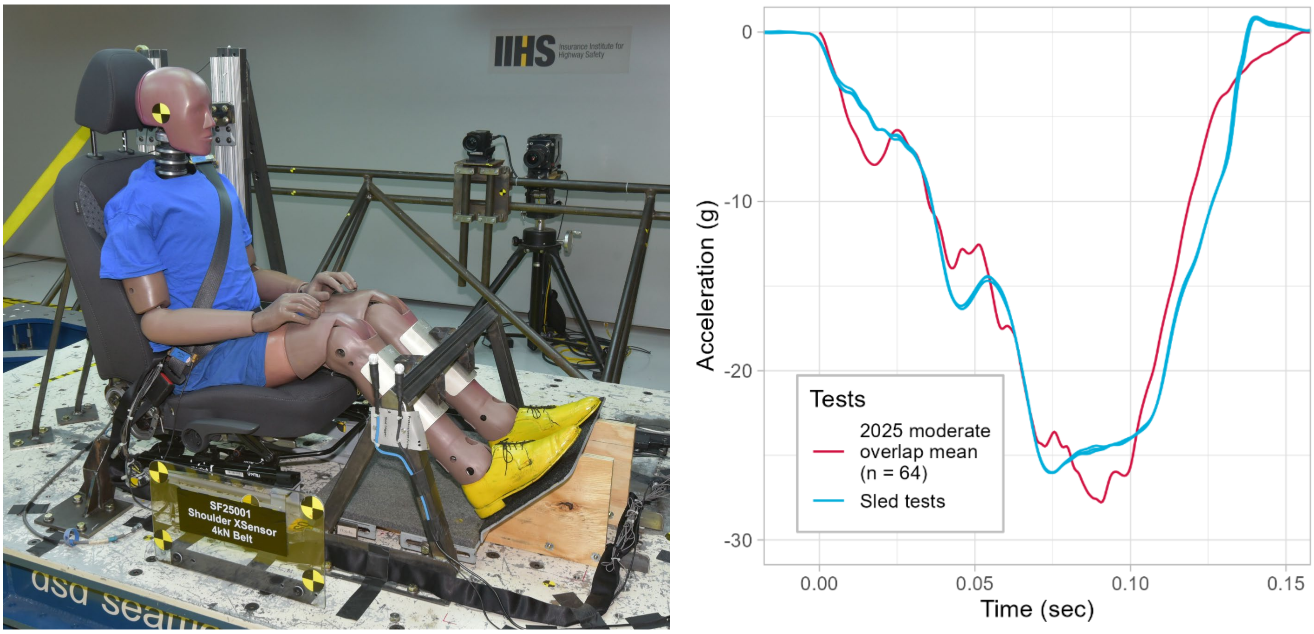

Fig. 1. Sled test with knee bolster (*left*) and sled pulse for all three tests compared with mean crash test pulse (*right*). Tests were conducted on a reverse acceleration sled; sled acceleration is inverted for comparison.

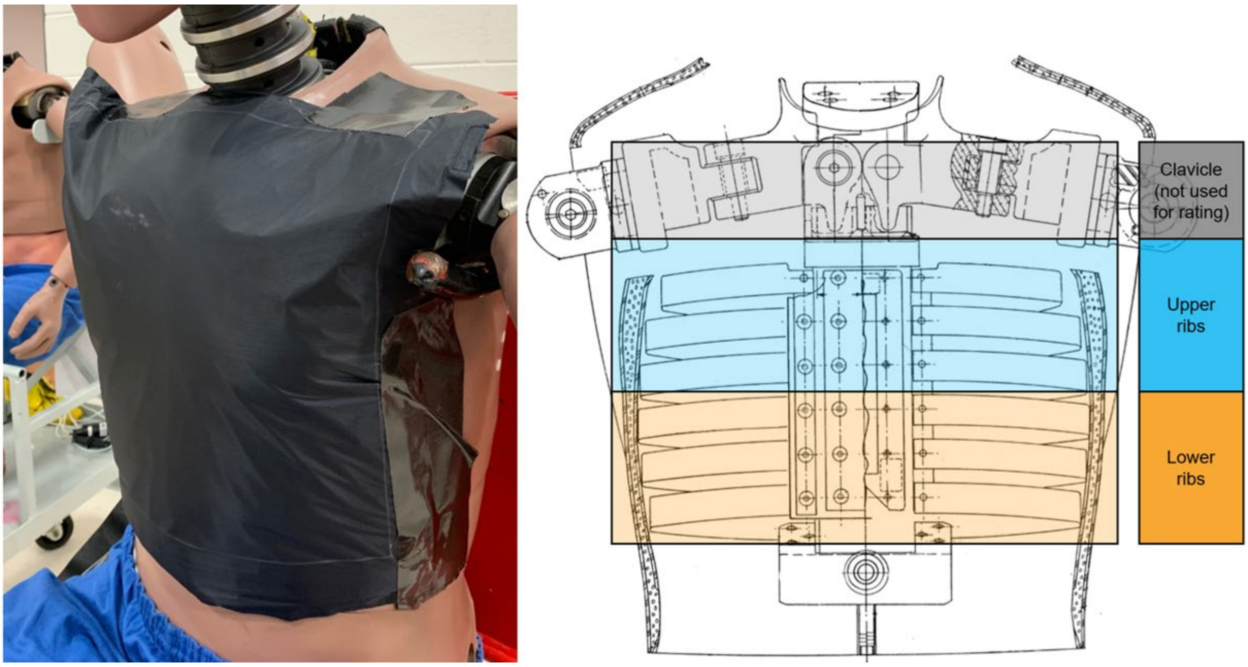

Fig. 2. XSensor pressure mat secured to dummy chest (*left*) and pressure-sensing area relative to underlying ribs (*right*).

Force Imbalance Metric

The proportion of the total force that occurs along the belt path could be used as a measure of restraint system load distribution, but it does not account for non-uniform forces by the seat belt or airbag across their loading areas, nor can it account for areas of the chest that are loaded by both the belt and airbag. To provide a more comprehensive assessment of the load distribution, a "force imbalance" metric was developed. At each time step, the force imbalance quantifies the degree to which a cumulative area vs cumulative force curve deviates from a perfectly even force distribution across the ribs.

To calculate the force imbalance at a specific time, the individual cell pressures p_i are first sorted in descending order so that $p_{(1)} \geq p_{(2)} \geq \cdots \geq p_{(N)}$. The total measured force is computed as:

$$F_{\text{tot}} = \sum_{i=1}^{N} p_i \, a \tag{1}$$

where a is the area of an individual cell, or 25.8 mm^2 for the XSensor mat used in this study. The full sensing area over the ribs A, was defined as 500 cm^2. While the actual area can vary somewhat as the ribs deform or the dummy orientation changes during the test, this value was treated as a constant to provide consistency throughout a test and between tests. For the cell ranked i, the cumulative area fraction is:

$$A_i = \frac{i\,a}{A} \tag{2}$$

and its cumulative force fraction is:

$$F_i = \sum_{k=1}^{i} \frac{p_{(k)}\,a}{F_{tot}} \tag{3}$$

The difference:

$$d_i = F_i - A_i \tag{4}$$

represents how much the cumulative force exceeds the cumulative area up to that point. The maximum value for d_i is the point where the cumulative force is most disproportionately concentrated relative to the area and is used to represent the overall force imbalance score at a given time. An example of the force calculation process is given in Appendix B.

Relative Force Imbalance

Since the force imbalance value changes throughout the test, a metric for characterising each test is needed. The maximum imbalance is not a meaningful characteristic value since it always occurs at low overall force levels. This is illustrated in Fig. 3 using an exemplar crash test. The chart on the left shows the time history of the XSensor rib force. The upper shoulder-belt tension is also shown for comparison. In the chart on the right, the force imbalance curve is plotted against the XSensor rib force. The imbalance was highest early and late in the test, when the ribs were loaded by a small area of the shoulder belt. As the dummy moved forward relative to the vehicle, more of the rib area was loaded during the "belt-only" phase, resulting in a slight reduction in the imbalance as the total force increased. However, the imbalance decreased most sharply relative to the rib force during combined loading from the shoulder belt and airbag. This illustrates the benefits of combined seat-belt and airbag loading: despite the increase in total rib force during this phase, the load is distributed more evenly across the rib cage. As a larger area of the chest is loaded, its effective stiffness increases, resulting in smaller deflections at the same total force level [8][19].

A linear reference was developed to serve as a fixed baseline that could be used to evaluate how well vehicle restraint systems manage the trade-off between force imbalance and force magnitude throughout a crash. The baseline is represented by the dashed line in Fig. 3 and has endpoints at 0 N (100% imbalance) and 7.5 kN (0% imbalance). It was defined using the mean slope for the combined loading phase from crash tests with at least 1 kN of loading from outside the belt path (n=37). For example, in the test shown in Fig. 3, the slope of the imbalance vs force line in the "combined" phase was −100% / 7986 N. The mean slope for all 37 tests was −100% / 7549 N. By using measurements from existing restraint systems rather than an arbitrary target, the baseline represents the expected behaviour of a hypothetical restraint system which provides typical benefits of combined loading, but which does so throughout the crash. In other words, a restraint system following the baseline behaviour would only increase total rib load by distributing that load more evenly across the ribs, even during the belt-only phase prior to airbag loading.

Once the combined loading baseline was established, a "relative imbalance" score for each test was calculated by taking the maximum difference between the imbalance–force curve and the baseline. For the example shown in Fig. 3, the maximum difference occurred at the point marked with an X (3311 N, 68%). This point was 12% above the baseline, indicating that purely combined loading would be expected to distribute similar forces over 12% more of the total rib area. In light of research indicating that pretensioner deployment is non-injurious [20], pre-tensioner loading was not used for calculating the relative imbalance. However, the maximum relative imbalance could occur at any other time during rib loading. In cases where the imbalance–force curve did not cross the baseline, the relative imbalance score is negative and indicates that the force was distributed over a relatively larger area than would be expected from a typical combined restraint system.

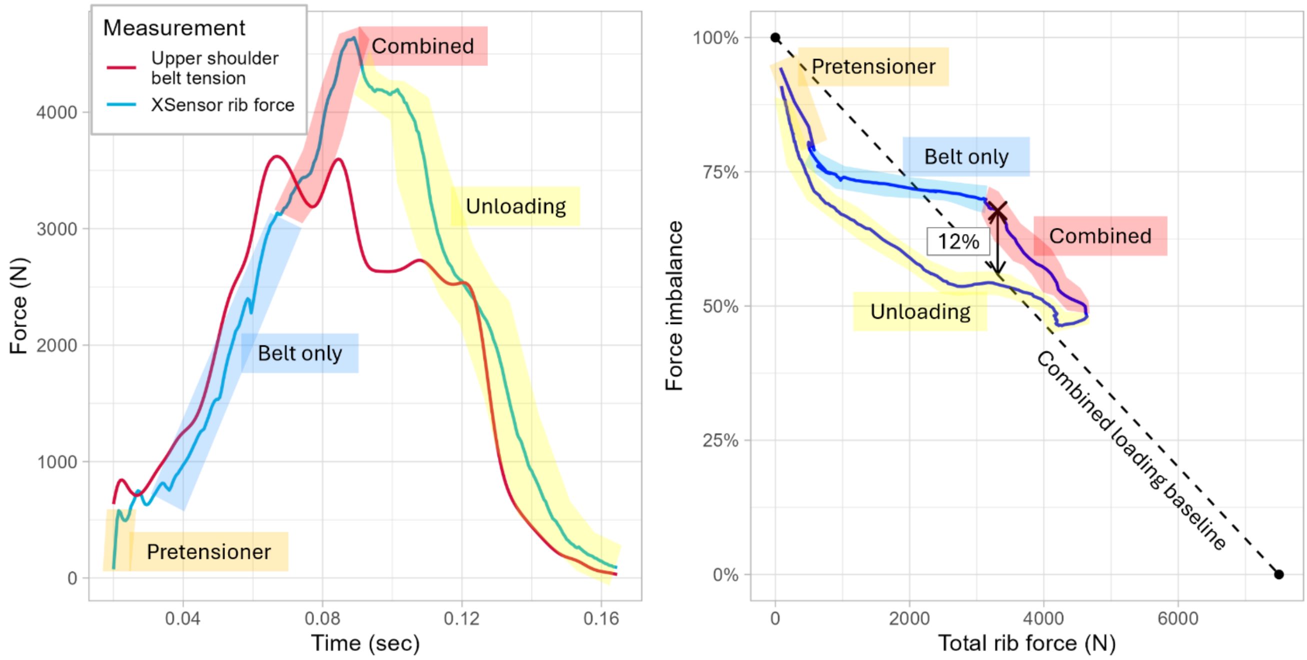

Fig. 3. Rib force and belt tension during loading phases in exemplar test (*left*) with resulting force imbalance (*right*). The dashed line in the right-hand chart indicates the combined loading baseline used to measure the relative imbalance for each test.

III. RESULTS

Figure 4 shows the maximum XSensor forces measured over different areas of the dummy ribs as well as the maximum upper shoulder-belt tension. For current-generation vehicles, the peak force over all ribs ranged from 2.4 kN to 5.9 kN, with a median of 4.0 kN. There was also a wide range of observed peak forces on the upper (1.6–3.6 kN) and lower (0.8–2.3 kN) ribs. The peak forces for the five older vehicle designs were usually greater than the 3rd quartile value from the newer vehicles for all ribs, as well as for the upper and lower ribs separately. Maximum forces over the different areas of the ribs did not always occur at the same time during the crash event, but were usually closely aligned.

Figure 5 (*left*) shows the range of relative imbalance scores, defined as the maximum imbalance relative to the combined loading baseline. The right-hand side of Fig. 5 shows the relationship between the force imbalance and total rib force at the time of the maximum relative imbalance. Pressure maps for two vehicles with different relative imbalance scores despite similar total rib force are shown in Fig. 6. Both vehicles produced peak rib force values of 3.9 kN, but this force was more concentrated for Vehicle A, as evidenced both by the larger areas of pressure exceeding 400 kPa and by the smaller areas of pressure between 100 kPa and 200 kPa.

Correlation coefficients for peak XSensor metrics, shoulder-belt tension, HIII sternum deflection, and thoracic acceleration are shown in Fig. 7 for the 82 tests of current-generation vehicles. The peak upper and lower rib forces were only weakly correlated ($r^2 = 0.28$). Compared with the upper rib force, the lower rib force was more strongly correlated with the force inside the belt path, peak shoulder-belt tension, and peak sternum deflection. As expected for a metric reflecting force distribution, relative imbalance was strongly correlated with the peak force inside the belt path and had a negative (though weak) correlation with force outside the belt path. Thoracic acceleration had only a weak correlation with all other metrics. Test-specific values are given in Appendix A along with other summary measures.

Sled test results for the XSensor force on the upper and lower ribs as well as the shoulder-belt tension are shown in Fig. 8. Other measures and video frames at maximum excursion are shown in Appendix C. Video analysis confirmed that the knee bolster limited femur and pelvis displacement to less than 2 cm relative to the sled. The shoulder-belt data indicate that the force limiters initiated belt spool-out close to their target thresholds. In the test with the 4 kN force limiter, the belt appeared to reach its maximum spool-out late in the test, resulting in increased tension. At around the same time, the lower ribs began loading the top of the thighs, further increasing the XSensor forces. Prior to this time, the two tests with a knee bolster produced similar forces on the lower ribs, but the belt tension difference was evident in the upper rib force. Conversely, in the two tests with similar belt tension, the presence of a knee bolster was associated with reduced force on the lower ribs but had a smaller effect on the upper rib force.

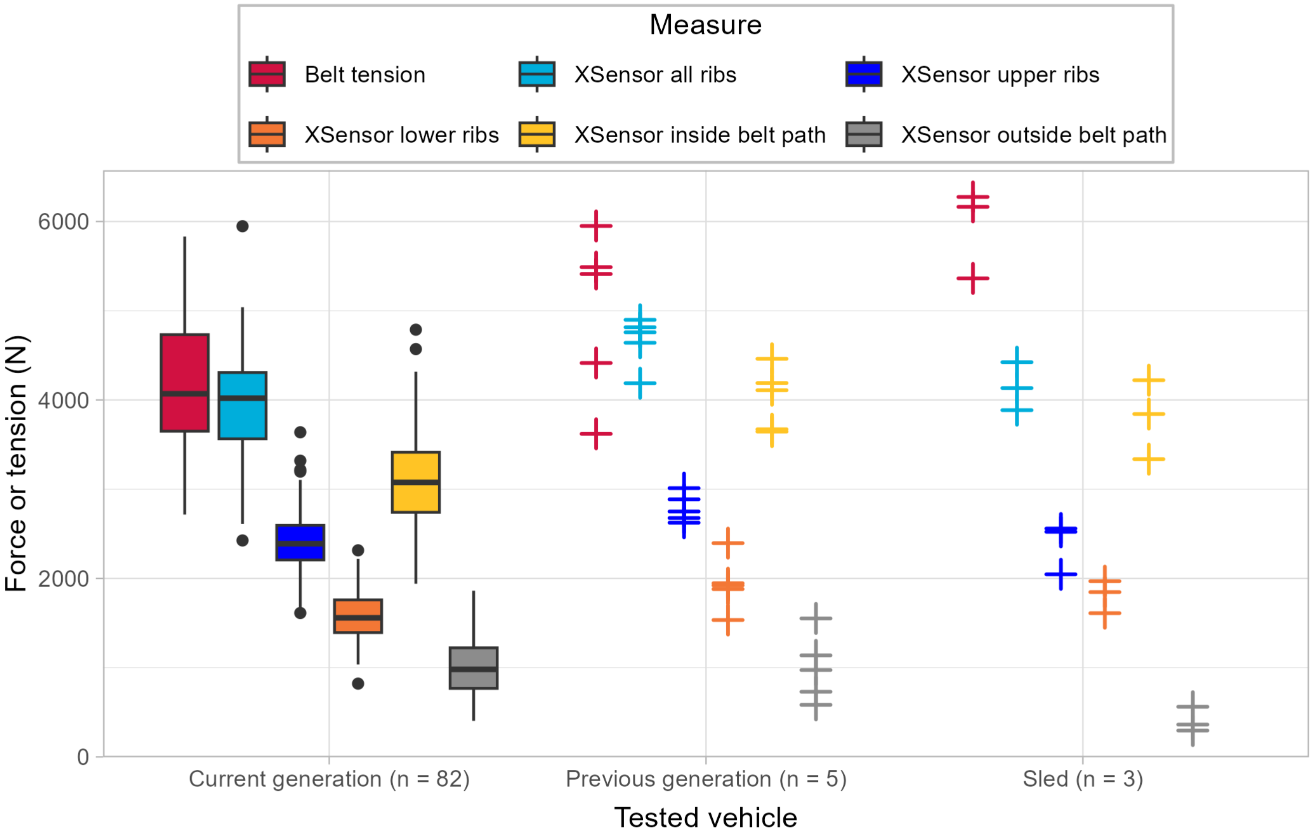

Fig. 4. Maximum values for upper shoulder-belt tension and XSensor forces over different areas.

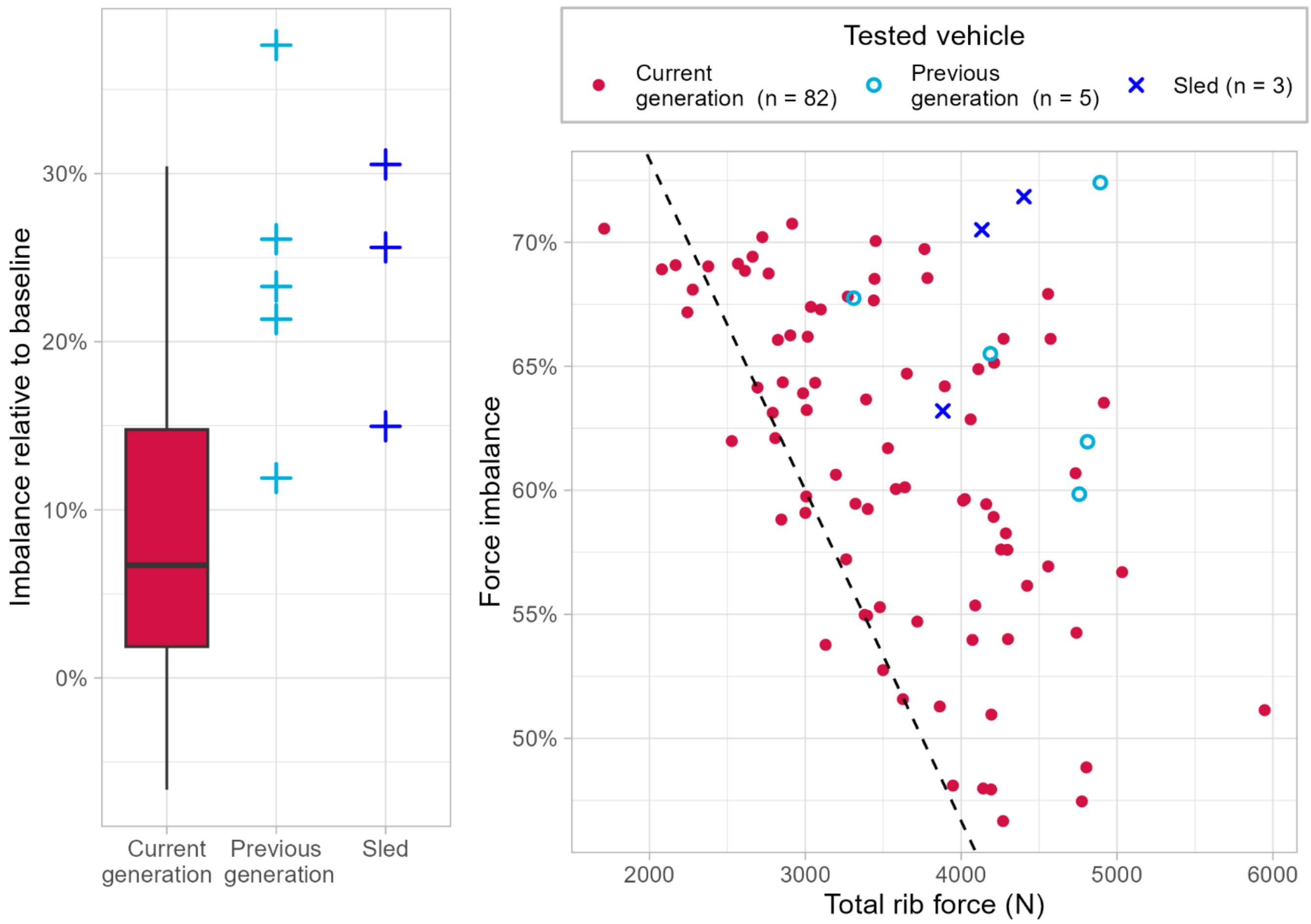

Fig. 5. Maximum relative imbalance scores (*left*) and imbalance vs force values at the time of maximum relative imbalance (*right*).

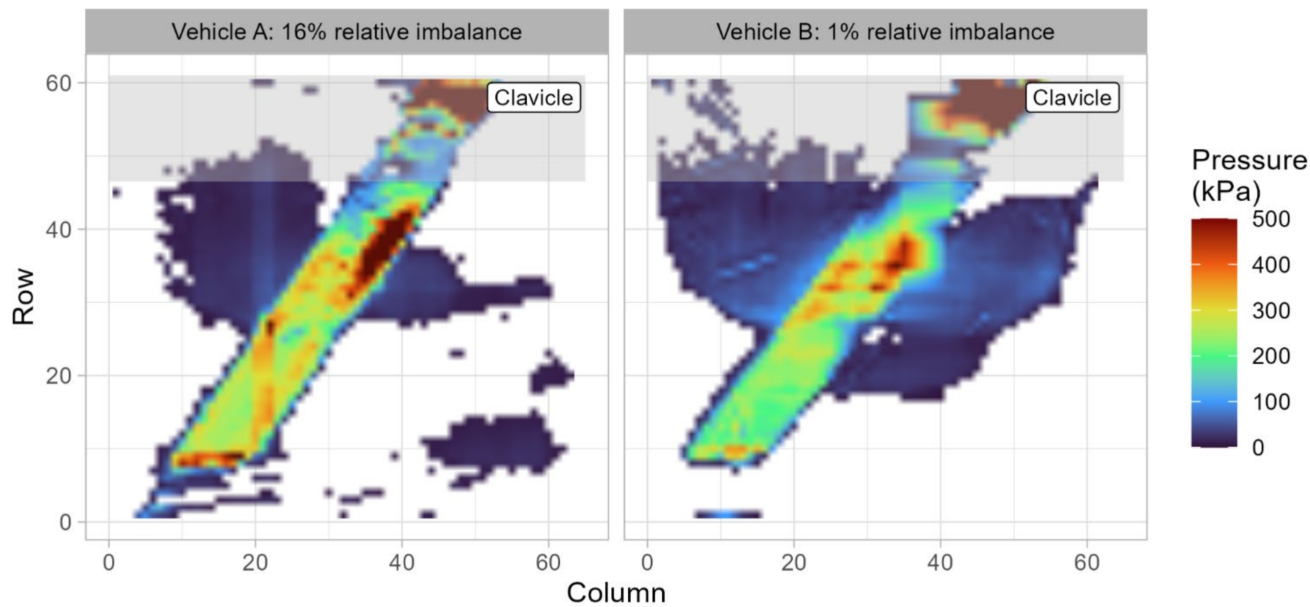

Fig. 6. Pressure maps for two tests at time of maximum relative imbalance.

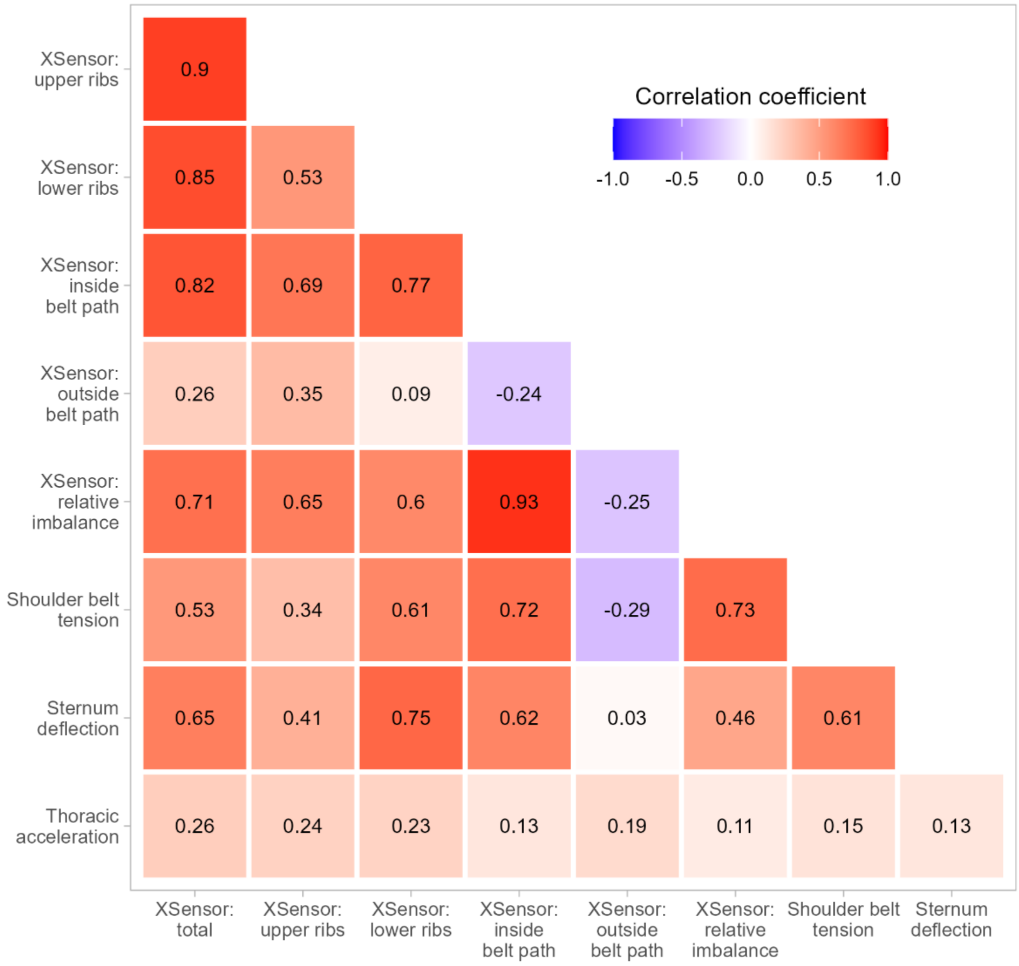

Fig. 7. Pearson correlation coefficients for maximum recorded values in tests of current production vehicles.

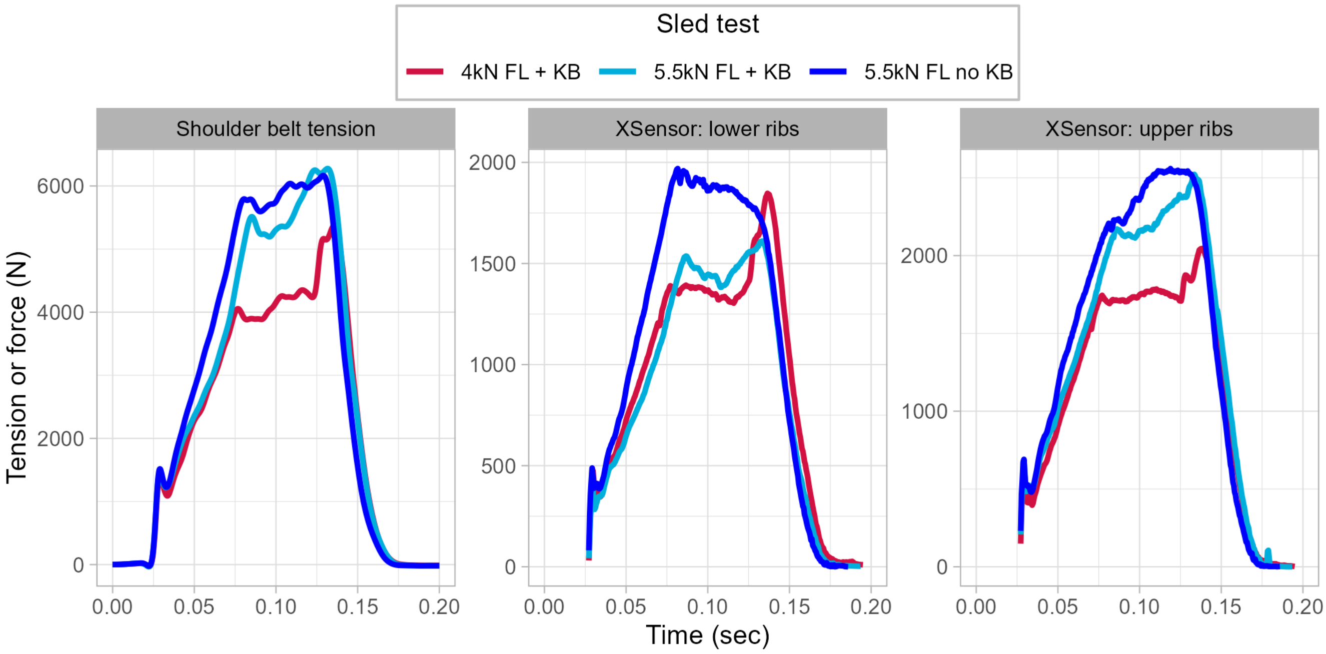

Fig. 8. Upper shoulder-belt tension and XSensor forces on lower and upper ribs in sled tests. *Note:* FL = force limiter; KB = knee bolster.

IV. DISCUSSION

This study demonstrates that high-speed pressure mat measurements can characterise how modern restraint systems load the HIII 50M chest in ways that conventional metrics cannot. Specifically, the pressure-derived measures quantify total rib loading, the distribution of the loading across the ribs, and the balance of the loading between the upper and lower ribs. Among current generation vehicles, there was a wide range of observed measures in peak total rib force, upper and lower rib forces, and in the evenness of the force distribution across the ribcage. In addition, the coefficient of variation for the force applied outside the belt path was much greater than that for other measures from the XSensor, dummy, or belt tension (Table AII). Together, these measures reveal differences in restraint strategies across contemporary vehicles that are obscured when relying on sternum deflection or shoulder-belt tension alone. More importantly, there are several indications that these differences have the potential to encourage restraint system designs that will better align with previously identified protection strategies.

The new force imbalance metric provides a means of quantifying how well the restraint system distributes loads across the ribcage in a way that has not been possible previously. While a completely balanced force distribution is unrealistic, the combined loading baseline offers a practical benchmark for evaluating how well a restraint system manages the trade-off between force magnitude and force distribution throughout the crash event. The relative imbalance score expresses how a given vehicle deviates from typical combined loading behaviour; positive values indicate more concentrated loading than expected, while negative values indicate better than typical distribution for the same rib force. While the relative imbalance score and the force inside the belt path were strongly correlated ($r = 0.93$; Fig. 7), the peak shoulder-belt tension had a weaker correlation with both ($r = 0.72$–0.73). This demonstrates one of the limitations of belt tension as a surrogate injury metric: the peak value can occur relatively early or late in the loading event with a resulting difference in concurrent airbag loading. The relative imbalance metric incorporates the full time history of pressure-mat data, capturing how well the belt and airbag timing, area, and stiffness characteristics are coordinated as the dummy interacts with the restraint system. While increased airbag loading will reduce the overall imbalance, if it is not well-matched with the belt tension phasing, the maximum relative imbalance may occur during an earlier “belt-only” loading phase. PMHS tests indicate a substantial number of rib fractures can occur relatively early in the event when belt tension is high but excursion into the airbag is minimal [21]. It should be noted that this study included vehicle-specific belt-path definitions in order to establish the combined loading baseline and to enable detailed comparisons between restraint systems, but that future use of the force imbalance metric itself does not require these definitions. Avoiding potentially subjective definitions is an advantage for any metric used in an evaluation program.

By considering only forces applied directly to the ribcage, the XSensor metrics inherently encourage alternative load paths, such as the clavicle and lower extremities. This is illustrated by the difference in the pair of sled tests that isolated the knee bolster effect, in particular by the force on the lower ribs, which was 18% lower in the test with the bolster. In this case, peak sternum deflection also was reduced (by 14%), and the deflection metric does provide some incentive for developing other load paths. However, rib loads applied laterally or vertically farther from the single measurement point of HIII-50M have the potential to reduce the apparent rib load without actually doing so [22]. In fact, PMHS testing indicates that loads applied laterally farther from the sternum produce greater deflection due to the lower degree of coupling at these locations [23]. In this way, the pressure mat data allow a more comprehensive analysis of ribcage loading, which, in turn, should promote more robust countermeasures to direct loads away from the chest.

The weak correlation between peak forces on the upper (superior) and lower (inferior) ribs ($r = 0.53$, Fig. 7) shows that there is some flexibility for restraint system designs to independently affect these regions and direct more load toward the stronger upper ribs [13], where fewer fractures are observed in the field data [10]. Once again, the sled tests provide a clear demonstration of this: the shoulder-belt force limiter primarily affected the upper rib force, and the knee bolster primarily affected the lower rib force (Fig. 8). In theory, criteria that have different thresholds for upper and lower rib forces could conflict with a force imbalance requirement. But in practice it is difficult to determine how much of a challenge this would create because the force on the lower ribs had almost no correlation with the force outside the belt path (Fig. 7). This is a possible explanation for the higher number of fractures observed at inferior rib locations [10]; in addition to being weaker, the lower rib cage benefits less from the combined loading effect offered by modern airbags that primarily load the head and upper torso. It will be important to monitor the effect of future restraint system developments on this behaviour. If field evidence continues to implicate inferior rib loading in severe injuries even with reduced forces, then it may be helpful to specify imbalance requirements that are specific to the lower ribs.

Relative to older designs, the current-generation vehicles had reduced ribcage loading overall. Only five older designs were tested, preventing definitive statements about changes in the fleet. However, it is interesting to note that the mean sternum deflection was only 8% lower for the newer vehicles, while the mean peak shoulder-belt tension was 16% lower (Table AII). The reductions in the mean pressure-derived measures of total rib force, upper rib force, and lower rib force (13–19%) were more consistent with the magnitude of the belt tension reduction. As belt tension has been shown to predict field crash outcomes better than sternum deflection [14][17], this alignment suggests that pressure-based metrics could be valuable for tracking and incentivising further chest-protection improvements.

Limitations

Several limitations warrant consideration. First, while the pressure-derived metrics described in the study are associated with established chest protection strategies, they have not been correlated directly with injury risk. Future work should evaluate their relationship to injury outcomes using human body models or by analysing field-crash data once a larger dataset of instrumented crash tests becomes available. All dummy-based evaluations have inherent limitations related to biofidelity and population diversity and it remains unknown to what degree these factors will restrict the applicability of pressure-derived measurements to the wider human population. Obtaining XSensor pressure data in PMHS tests could provide an even stronger link to human injury tolerance and the most effective protection strategies [24]. Second, the pressure mat used in this study was not specifically designed for the HIII-50M dummy. A version tailored to the dummy's shape would likely improve repeatability and placement consistency. Additionally, a certification protocol is needed before the pressure mat data can be used in a vehicle evaluation program. Such a protocol should verify that mat output corresponds to known force standards and ensure that calibrations remain stable across tests. In this study, two different sensors were used and recalibrated multiple times, underscoring the need for a standardised procedure. Third, the present analysis was conducted using a single dummy size and one frontal test mode. Generalisation to other occupant sizes, seating positions, and frontal configurations (e.g. small overlap) remains to be evaluated. In addition, comparable pressure mat data using THOR could allow further insights into the different response of the dummies to combined belt and airbag loading.

V. CONCLUSION

High-speed pressure mat measurements can quantify important aspects of driver chest loading in frontal crash tests that are not captured by existing dummy metrics. The XSensor system provided direct measures of total rib force and the relative loading of the upper and lower ribs. In addition, the newly developed relative imbalance score offers a means of quantifying how restraint systems manage the trade-off between load magnitude and load distribution throughout the loading event. Together, these measures revealed substantial variation in restraint system behaviour among modern designs and are well-aligned with previously identified strategies – distributing loads more evenly across the ribs, utilising alternative load paths, and reducing total force on the weaker lower ribs. The XSensor pressure mat is a promising tool for future chest injury assessment in frontal crashworthiness evaluations.

VI. ACKNOWLEDGMENTS

The author is grateful for the generous loan of sensors and expert technical support provided by XSENSOR Technology Corporation, in particular from Tim Gorjanc, Greg Fukushima and Karl Schilling. The study would not have been feasible without the dedication and professionalism of the crash test team at the IIHS Vehicle Research Center.

VII. REFERENCES

[1] Insurance Institute for Highway Safety (2023) *Fatality facts 2023*. Available: https://www.iihs.org/research-areas/fatality-statistics.

[2] Brumbelow, M. L. (2019) Front crash injury risks for restrained drivers in good-rated vehicles by age, impact configuration, and EDR-based delta V. *Proceedings of the IRCOBI Conference,* 2019, Florence, Italy.

[3] Farmer, C. M. (2005) Relationships of frontal offset crash test results to real-world driver fatality rates. *Traffic Injury Prevention*, **6**(1): pp. 31–37.

[4] Teoh, E. R, Monfort S. S. (2023) IIHS small overlap frontal crash test ratings and real-world driver death risk. *Traffic Injury Prevention*, **24**(5): pp. 409–413.

[5] Brumbelow, M. L, Jermakian, J. S. (2022) Injury risks and crashworthiness benefits for females and males: Which differences are physiological? *Traffic Injury Prevention*, **23**(1): pp. 11–16.

[6] Kallieris, D., Rizzetti, A., *et al*. (1995) On the synergism of the driver air bag and the 3-point belt in frontal collisions. *SAE Transactions*, **104**: pp. 2857–2869.

[7] Petitjean, A., Lebarbe, M., Potier, P., Trosseille, X., Lassau, J. P. (2002) Laboratory reconstructions of real-world frontal crash configurations using the Hybrid III and THOR dummies and PMHS. *Stapp Car Crash Journal*, **46**: pp. 27–54.

[8] Kent, R., Sherwood, C., Lessley, D., Overby, B., Matsuoka, F. (2003) Age-related changes in the effective stiffness of the human thorax using four loading conditions. *Proceedings of IRCOBI Conference*, 2003, Lisbon, Portugal.

[9] Brumbelow, M. L. (2024) Reassessing PMHS rib fractures in front sled tests to improve modern restraint systems. *Proceedings of the IRCOBI Conference*, 2024, Stockholm, Sweden.

[10] Brumbelow, M. L. (2024) Identifying thoracic injury factors by comparing rib fracture patterns in field crashes and PMHS sled tests. *Proceedings of the IRCOBI Conference*, 2024, Stockholm, Sweden.

[11] McMurry, T. L., Forman, J. L., Shaw, G., Crandall, J. R. (2019) Evaluating the influence of knee airbags on lower limb and whole-body injury. *Traffic Injury Prevention*, **21**(1): pp. 72–77.

[12] Rouhana, S. W., Bedewi, P. G., *et al*. (2003) Biomechanics of 4-point seat belt systems in frontal impacts. *Stapp Car Crash Journal*, **47**: pp. 367–399.

[13] Kindig, M. W., Lau, A. G., Forman, J. L., Kent, R. W. (2010) Structural response of cadaveric ribcages under a localized loading: Stiffness and kinematic trends. *Stapp Car Crash Journal*, **54**: pp. 337–380.

[14] Brumbelow, M. L. (2020) Can front crash rating programs using Hybrid III predict real-world thoracic injuries? *Proceedings of the IRCOBI Conference*, 2020, (online).

[15] Insurance Institute for Highway Safety (2023) Submission to NHTSA docket. NPRM anthropomorphic test devices: Test device for Human Anthropomorphic Test Devices: Test device for human occupant restraint 50th percentile adult male test dummy; Incorporation by Reference.

[16] Brumbelow, M. L., Farmer, C. F. (2013) Real-world injury patterns associated with Hybrid III sternal deflections in frontal crash tests. *Traffic Injury Prevention*, **14**(9): pp. 807–815.

[17] Brumbelow, M. L, Jermakian, J. S, Arbelaez, R. A. (2022) Predicting real-world thoracic injury using THOR and Hybrid III crash tests. *Proceedings of the IRCOBI Conference*, 2022, Porto, Portugal.

[18] Insurance Institute for Highway Safety (2023) Moderate overlap frontal testing 2.0 crash test protocol: Version I. Available: https://www.iihs.org/ratings/about-our-tests/test-protocols-and-technical-information.

[19] Schneider, L. W., King, A. I., Beebe, M. S. (1989) Design requirements and specifications: Thorax-abdomen development task; interim report; trauma assessment device development program. U.S. Department of Transportation Report No. DOT HS 807 511.

[20] Bolte, J. B., Linton, E., Kang, Y. S., Agnew, A. (2025) Defining a non-injurious load case for small female ATDs based on PMHS tests. *Proceedings of the IRCOBI Conference*, 2025, Vilnius, Lithuania.

[21] Albert, D. L., Beeman, S. M., Kemper, A. R. (2018) Assessment of thoracic response and injury risk using the Hybrid III, THOR-M, and post-mortem human surrogates under various restraint conditions in full-scale frontal sled tests. *Stapp Car Crash Journal*, **62**: pp. 1–65.

[22] Mizuno, K., Nezaki, S., Ito, D. (2017) Comparison of chest injury measures of Hybrid III dummy. *International Journal of Crashworthiness*, **22**(1), pp. 38–48.

[23] Shaw, G., Lessley, D., *et al*. (2007) Quasi-static and dynamic thoracic loading tests: Cadaveric torsos. *Proceedings of the IRCOBI Conference*, 2007, Maastricht, the Netherlands.

[24] Bolte, J. B., Van Meter, M., *et al.* (2022 XSENSOR high-speed impact system in PMHS thoracic impact testing. *Proceedings of the IRCOBI Conference,* 2022, Porto, Portugal.

VIII. APPENDIX

APPENDIX A: XSENSOR CRASH TESTS

TABLE AI
INDIVIDUAL RESULTS

Test ID	Vehicle	Total rib force (N)	Upper rib force (N)	Lower rib force (N)	Relative imbalance
	Current-generation vehicles				
CEF2103	2021 Buick Encore	4469	2917	1556	10%
CEF2107	2022 Mitsubishi Eclipse Cross	4161	2819	1344	15%
CEF2108	2021 Volvo XC40	4847	3319	1548	29%
CEF2110	2021 Toyota RAV4	4304	2579	1748	15%
CEF2111	2021 Honda HR-V	4064	2691	1393	17%
CEF2113	2021 Subaru Forester	4734	2850	1900	24%
CEF2114	2021 Ford Escape	4791	3197	1609	20%
CEF2115	2021 Honda CR-V	4824	3218	1612	13%
CEF2116	2021 Chevrolet Equinox	4902	3104	1805	8%
CEF2118	2021 Jeep Renegade	5947	3638	2315	30%
CEF2208	2022 Subaru Ascent	4920	2726	2219	29%
CEF2230	2022 Tesla Model Y	3511	2363	1215	3%
CEF2322	2023 Acura MDX	4240	2714	1540	4%
CEF2323	2023 Audi Q5	4313	2462	1885	15%
CEF2325	2023 Cadillac XT6	3947	2528	1421	1%
CEF2326	2023 Lincoln Aviator	3720	2379	1347	16%
CEF2327	2023 Volvo XC60	4059	2582	1496	19%
CEF2328	2023 Lexus RX	3746	2285	1471	4%
CEF2329	2023 Ram 1500 (crew cab)	3242	2283	1036	7%
CEF2330	2022 Jeep Grand Cherokee L	4272	2548	1746	23%
CEF2331	2023 Ford Maverick (crew cab)	4055	2439	1636	14%
CEF2332	2023 Ford F-150 (crew cab)	3147	2010	1158	4%
CEF2333	2023 Kia Telluride	4775	2897	1878	11%
CEF2334	2024 Mercedes-Benz GLE 350	5039	2937	2121	24%
CEF2335	2023 Subaru Legacy	4760	2742	2018	17%
CEF2336	2023 Lexus ES 350	4174	2719	1488	13%
CEF2337	2023 Lexus UX	4179	2490	1699	3%
CEF2338	2023 Hyundai Ioniq 6	4194	2510	1686	7%
CEF2339	2023 Toyota Prius	3859	2322	1538	9%
CEF2340	2023 Toyota Venza	3875	2254	1658	9%
CEF2341	2023 Toyota Corolla Cross	3634	2220	1433	0%
CEF2342	2024 Mazda CX-90	3594	2248	1353	0%
CEF2343	2024 Honda CR-V	3201	2268	1125	0%

TABLE AI

INDIVIDUAL RESULTS

Test ID	Vehicle	Total rib force (N)	Upper rib force (N)	Lower rib force (N)	Relative imbalance
CEF2344	2024 Honda HR-V	3650	2507	1148	11%
CEF2345	2024 Acura Integra	3656	2559	1124	6%
CEF2346	2024 Hyundai Kona	4124	2552	1580	14%
CEF2347	2024 Genesis GV60	3686	2267	1423	0%
CEF2348	2024 Mazda CX-30	4230	2615	1665	3%
CEF2349	2024 Mazda CX-50	4073	2446	1642	8%
CEF2350	2024 Mazda 3 (hatchback)	3813	2261	1554	0%
CEF2351	2024 Mazda 3 (sedan)	3577	2196	1462	2%
CEF2402	2024 Genesis GV70	4003	2431	1585	-2%
CEF2403	2024 Genesis GV80	3561	2350	1221	-3%
CEF2404	2024 Hyundai Elantra	4037	2308	1735	5%
CEF2405	2023 Jeep Wagoneer	2426	1640	821	-7%
CEF2406	2024 Ford Expedition	3545	2096	1452	9%
CEF2407	2023 Chevrolet Tahoe	3487	2103	1390	-1%
CEF2409	2024 Genesis G80	4309	2614	1695	11%
CEF2410	2024 Genesis Electrified G80	3513	2139	1395	4%
CEF2411	2024 Genesis G90	4370	2564	1829	-3%
CEF2412	2024 Hyundai Ioniq 5	3587	2113	1474	-3%
CEF2413	2024 Nissan Pathfinder	3656	2202	1457	13%
CEF2414	2024 Rivian R1T	4237	2399	1932	21%
CEF2416	2024 Hyundai Santa Fe	3901	2343	1561	0%
CEF2417	2024 Subaru Crosstrek	4562	2462	2108	18%
CEF2418	2024 Subaru Impreza	3919	2280	1664	16%
CEF2419	2024 Lincoln Nautilus	3128	2008	1146	3%
CEF2420	2024 Mazda CX-5	4263	2317	1946	14%
CEF2421	2024 Nissan Altima	4366	2892	1580	15%
CEF2422	2024 Lexus NX	4476	2506	1970	5%
CEF2423	2024 Mazda CX-90 PHEV	3553	2126	1436	0%
CEF2424	2025 Honda Pilot	3868	2323	1577	5%
CEF2426	2024 BMW X5	4463	2600	1899	15%
CEF2428	2024 Hyundai Santa Cruz	4045	2535	1517	1%
CEF2429	2024 Hyundai Tucson	4588	2707	1906	2%
CEF2436	2025 Subaru Forester	2978	1884	1131	4%
CEF2443	2024 Mercedes-Benz C 300	3527	2241	1292	1%
CEF2444	2024 Mercedes-Benz GLC 300	4270	2339	1938	4%
CEF2445	2025 Mazda CX-70	3250	1801	1461	-4%
CEF2446	2025 Mazda CX-70 PHEV	3198	2019	1185	3%
CEF2447	2025 Rivian R1S	4477	2452	2025	20%
CEF2448	2025 Rivian R1T	4623	2638	1985	27%
CEF2449	2024 Volvo XC90 Recharge	3792	2073	1764	6%
CEF2450	2025 Kia Sorento	3427	2151	1294	-2%
CEF2451	2024 Cadillac Lyriq	3499	2177	1377	-1%

TABLE AI
INDIVIDUAL RESULTS

Test ID	Vehicle	Total rib force (N)	Upper rib force (N)	Lower rib force (N)	Relative imbalance
CEF2453	2024 Toyota bZ4X	3550	1961	1599	9%
CEF2454	2025 Toyota Tundra (crew cab)	4126	2448	1685	10%
CEF2456	2025 Infiniti QX80	2611	1612	1088	-4%
CEF2457	2025 Hyundai Palisade	3946	2123	1824	8%
CEF2502	2025 Audi Q7	4226	2366	1874	13%
CEF2504	2024 Chevrolet Traverse	3470	2040	1431	4%
CEF2508	2025 Hyundai Elantra	3522	2202	1349	5%
	Prior-generation vehicles				
CF21012	2004 Honda Civic 4-door	4815	3012	1922	26%
CF21013	2010 Ford Focus 4-door	4758	2886	1880	23%
CF21014	2006 Toyota Highlander	4898	2625	2396	38%
CF21015	2011 Volvo XC90	4641	2750	1947	12%
CF21016	2012 Nissan Altima	4188	2677	1534	21%

TABLE AII
SUMMARY RESULTS

	Min.	Max.	Median	Mean	Standard deviation	Coefficient of variation
Current generation (n=82)						
XSensor: total rib force (N)	2426	5947	4020	3984	577	0.14
XSensor: upper rib force (N)	1612	3638	2389	2430	355	0.15
XSensor: lower rib force (N)	821	2315	1559	1576	294	0.19
XSensor: inside belt path (N)	1941	4788	3076	3132	546	0.17
XSensor: outside belt path (N)	404	1863	981	1012	318	0.31
Sternum deflection (mm)	16.7	36.3	27.1	27.0	4.2	0.16
Thoracic acceleration (g)	23.8	44.9	34.7	34.7	4.9	0.14
Shoulder-belt tension (N)	2716	5832	4069	4174	747	0.18
Previous generation (n=5)						
XSensor: total rib force (N)	4188	4898	4758	4660	280	0.06
XSensor: upper rib force (N)	2625	3012	2750	2790	158	0.06
XSensor: lower rib force (N)	1534	2396	1922	1936	307	0.16
XSensor: inside belt path (N)	3645	4461	4109	4015	351	0.09
XSensor: outside belt path (N)	584	1552	974	995	378	0.38
Sternum deflection (mm)	25.7	33.2	29.3	29.2	2.7	0.09
Thoracic acceleration (g)	37.2	45.9	41.1	40.6	3.6	0.09
Shoulder-belt tension (N)	3621	5950	5412	4977	943	0.19

APPENDIX B: FORCE IMBALANCE EXAMPLE

Figure B1 shows an example of the force imbalance calculation process. At this time step, there were 1,472 cells with recorded pressure, excluding the cells over the clavicle and shoulder assembly. The maximum cell-level pressure was 759 kPa, which equates to a force of 19.6 N, and the smallest was 7 kPa (0.2 N). The total force over all cells was 5,521 N. The cells are ranked in descending order of pressure, with the 10 cells with the highest pressure labelled in Fig. B1.

With the cells in rank order, the cumulative force was calculated and converted to a percentage of the total rib area of 500 cm^2. The solid curve in Fig. B2 indicates the cumulative force vs cumulative area line. A force that was evenly distributed across the entire rib area would produce a curve that falls on the dashed line. In this example case, the maximum deviation from an evenly distributed load was represented by the 496 cells with the greatest pressure, which accounted for 80% of the total load and 26% of the total rib area. The difference of 54% is defined as the force imbalance at this point in the test.

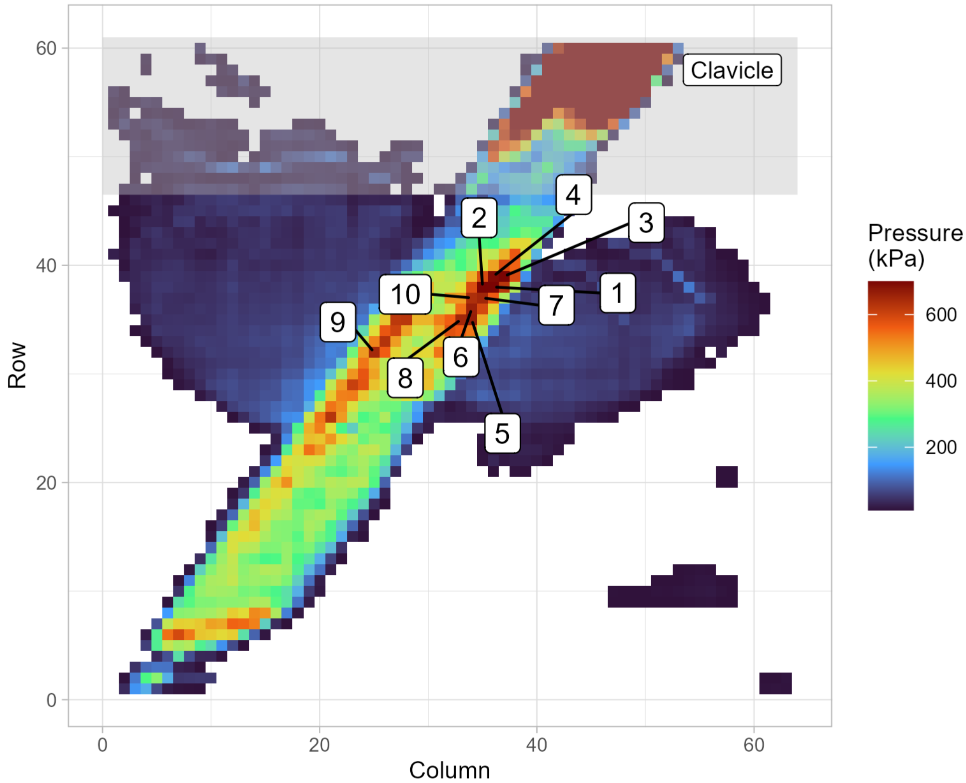

Rank	Pressure (kPa)	Force (N)	Cumulative force (N)	Total force (N)	Cumulative force (%) (Eq 3)	Cumulative area (cm²)	Cumulative area (%) (Eq 2)	Imbalance: cumulative force minus area (%) (Eq 4)
1	759	19.6	19.6	5531	0.35	0.26	0.05	0.3
2	736	19	38.6	5531	0.7	0.52	0.1	0.59
3	708	18.3	56.9	5531	1.03	0.77	0.15	0.87
...	...	...	...	...	...	...	...	...
495	111	2.9	4417.8	5531	79.87	127.74	25.55	54.32
496	111	2.9	4420.7	5531	79.92	128	25.6	54.32
497	111	2.9	4423.5	5531	79.97	128.26	25.65	54.32
...	...	...	...	...	...	...	...	...
1472	7	0.2	5531.2	5531	100	379.87	75.97	24.03

Fig. B1. Pressure map with labels showing top 10 highest pressure cells and calculated values for cumulative force, area, and imbalance (force minus area). Equation numbers reference those in the text.

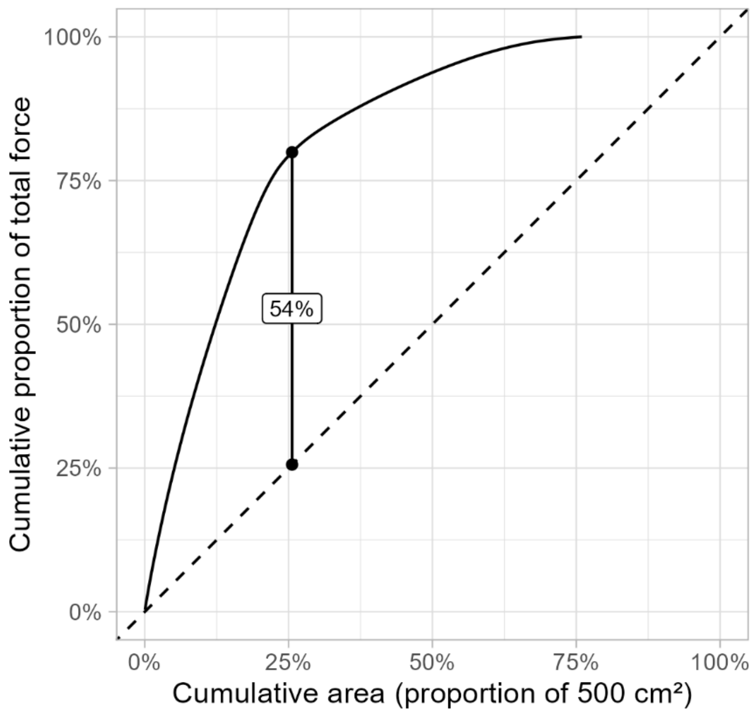

Fig. B2. Cumulative proportion of force vs cumulative proportion of area, with imbalance defined as the maximum difference.

APPENDIX C: ADDITIONAL SLED TEST RESULTS

Figure C1 shows the imbalance vs force, sternum deflection, and Y-axis rotation recorded by an angular rate sensor mounted at the dummy's T4 location. Figure C2 shows the dummy position at the time of maximum rotation. As discussed in the results, the dummy's rotation in the 4 kN force limiter test allowed the lower ribs to contact the top of the thighs. This is evident in the imbalance vs force curve (left side of Fig. C1), which showed reduced imbalance between 3.0 kN and 4.0 kN of rib force. The thigh loading is also evident in Fig. C3, which shows the pressure map for each test at the time of maximum total rib force.

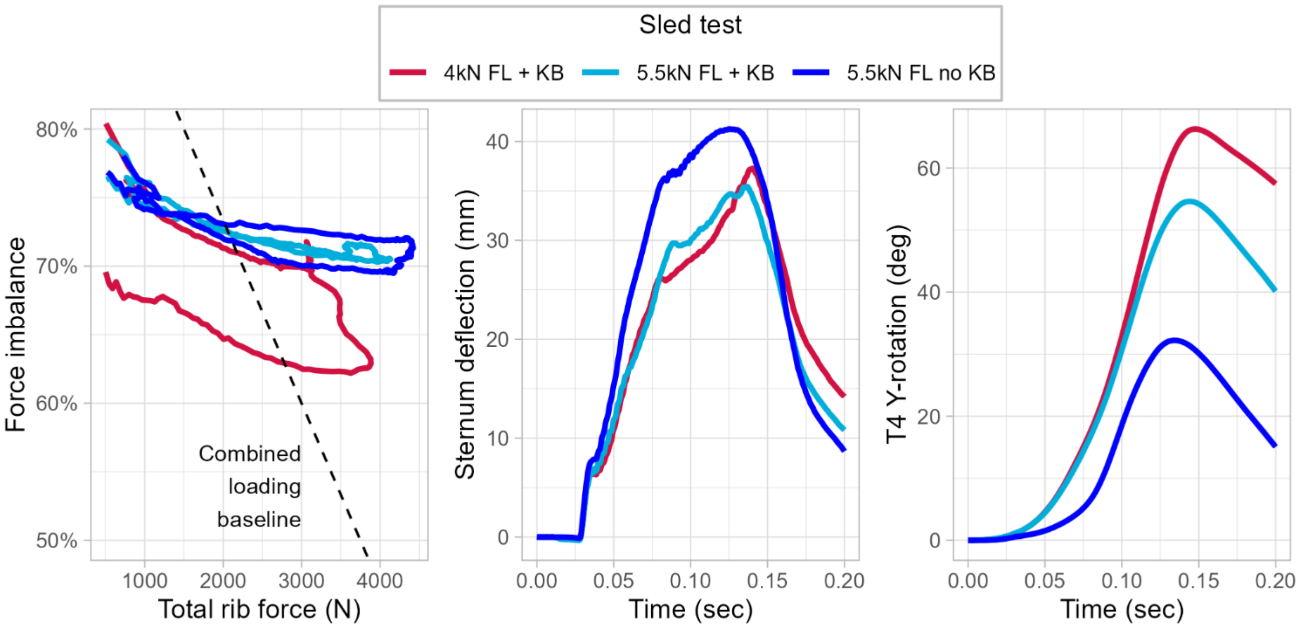

Fig. C1. Sled test results for imbalance vs force, sternum deflection and torso rotation measured at T4.
Note: FL = force limiter; KB = knee bolster.

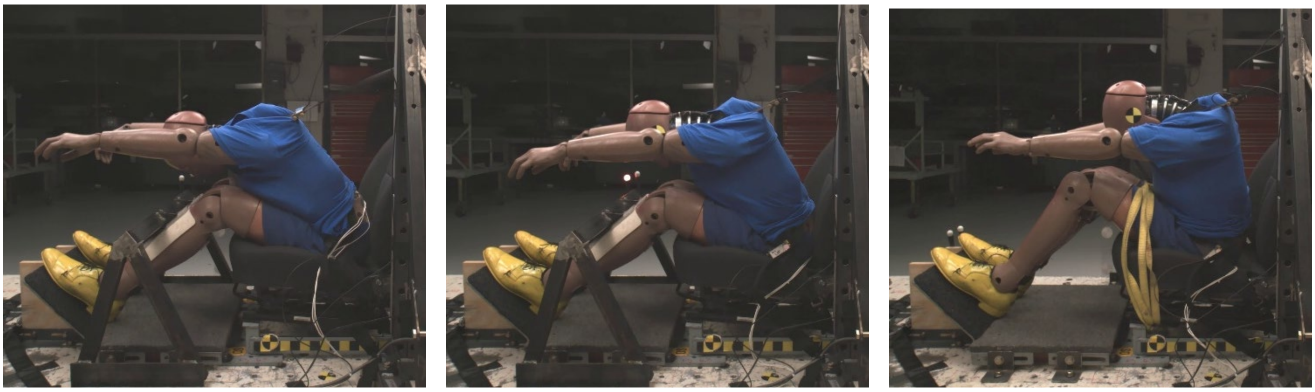

Fig. C2. Sled test video frames at time of maximum torso rotation. Test conditions from left to right: 4 kN force limiter with knee bolster, 5.5 kN force limiter with knee bolster, 5.5 kN force limiter without knee bolster.

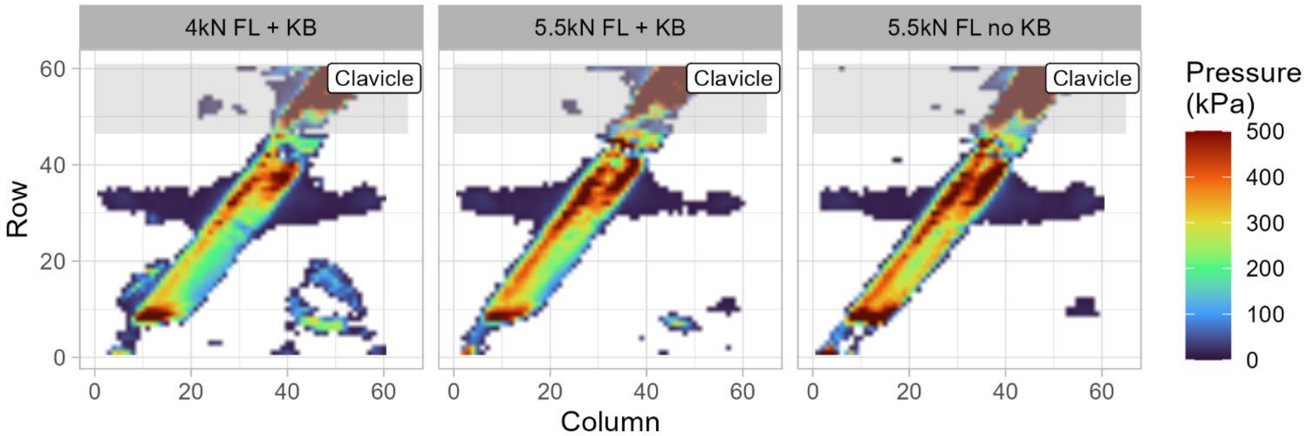

Fig. C3. Sled test pressure maps at time of maximum total rib force. *Note:* FL = force limiter; KB = knee bolster.